$$\sqrt{\rho'^2}/\bar{\rho} = (c_f/2)^{1/2}(\bar{\rho}u'^2/\tau_w)^{1/2} \times [r(\gamma-1)M_e^2(\bar{u}/u_e - 1/2) + (T_w/T_e - 1)]/(\bar{T}/T_e)^{1/2} \quad (5)$$

The temperature distributions in Eqs. (4) and (5) are given by Eqs. (1) and (2), respectively.

Results and Discussion

Sources were located that report experimentally determined local density fluctuation profiles for adiabatic-wall[11,12] and nonadiabatic-wall[12-14] turbulent boundary layers. The reported experimental values for c_f, M_e, T_w/T_e, T_e, and Reynolds normal stress ($\bar{\rho}u'^2$) were used in Eqs. (4) and (5). The temperature profiles were computed from a 1/7th-power law velocity profile.

A comparison among Eq. (4) and the experimental data[11,12] for three supersonic boundary layers is shown in Fig. 1. At a fixed y/δ, the model and data increase for increasing M_e. The data and predicted values show a maximum in the midportion of the boundary layer. The model is observed to adequately predict the quantitative behavior in supersonic adiabatic-wall boundary layers.

A comparison among Eq. (5) and the experimental data[12-14] for nonadiabatic boundary layers is shown in Fig. 2. Quantitative agreement among data and model predictions is less favorable than the adiabatic case. The predicted values show a maximum. This trend is in qualitative agreement with the data.

The quantity subject to the greatest computational and measurement uncertainty in the present model is the Reynolds normal stress. The predicted values shown in Figs. 1 and 2 have the same uncertainty as those used in the model calculations. All Reynolds normal stress and density fluctuation data reported herein were obtained from thermal anemometry measurements. It is noted that thermal anemometry measurements can result in erroneously low readings if not properly frequency-compensated.[12] Improper compensation usually results in attenuation of the high-frequency component of the signal. Exact compensation is difficult to achieve since the hot-wire "constants" are functions of the position within the boundary layer. In hypersonic boundary layers, the measured velocity fluctuations are strongly dependent upon the total temperature fluctuations. Total temperature fluctuation measurements can show significant scatter (e.g., see Ref. 13). The aforementioned arguments may explain the large scatter among the nonadiabatic wall data and predicted values shown in Fig. 2. Additional measurements of the Reynolds normal stress and density fluctuations are needed to establish the data trends in the boundary layer.

Conclusions

A model for predicting the local density fluctuations in supersonic turbulent boundary layers is proposed. The model is based upon the differential form of the Crocco-Busemann temperature solutions and negligible pressure fluctuations. Model results were compared against adiabatic-wall, supersonic turbulent boundary-layer data, and showed good agreement. Model results are unable to adequately predict the quantitative behavior of nonadiabatic-wall, turbulent boundary-layer data.

Acknowledgment

The reported research was performed under Task ZJSO of Contract N00039-87-C-5301 with the Space and Naval Warfare Systems Command and was sponsored by and under the technical cognizance of the U.S. Army Strategic Defense Command.

References

[1]Gilbert, K. G. and Otten, L. J. (eds.), *Progress in Astronautics and Aeronautics: Aero-Optical Phenomena,* Vol. 80, AIAA, New York, 1982.

[2]Sutton, G. W., "Aero-Optical Foundations and Applications," *AIAA Journal,* Vol. 23, Oct. 1985, pp. 1525-1537.

[3]Sutton, G. W., "Optical Imaging Through Aircraft Boundary Layers," *Progress in Astronautics and Aeronautics,* Vol. 80, AIAA, New York, 1982, pp. 15-39.

[4]Kelsall, D., "Optical Measurements of Degradation in Aircraft Boundary Layers," *Progress in Astronautics and Aeronautics,* Vol. 80, AIAA, New York, 1982, pp. 261-293.

[5]White, F. M., *Viscous Fluid Flow,* McGraw-Hill, New York, 1974.

[6]Morkovin, M. V., *The Mechanics of Turbulence,* edited by A. Favre, Gordon and Breach, New York, 1964.

[7]Morkovin, M. V., "AGARD Wind Tunnel and Model Testing Panel," Harford House, London, 1960.

[8]Bradshaw, P. (ed.), *Turbulence,* Springer-Verlag, New York, 1976, pp. 91-97.

[9]Bradshaw, P., "Compressible Turbulent Shear Layers," *Annual Review of Fluid Mechanics,* Vol. 9, Annual Reviews, Inc., Palo Alto, CA, 1977, pp. 33-54.

[10]Kovasznay, L. S. G., "Hot Wire Anemometer in Supersonic Flow," *Journal of Aeronautical Science,* Vol. 17, Sept. 1950, pp. 565-572.

[11]Kistler, A. L., "Fluctuation Measurements in a Supersonic Turbulent Boundary Layer," *Physics of Fluids,* Vol. 2, No. 3, 1959, pp. 290-296.

[12]Laderman, A. J. and Demetriades, A., "Turbulent Shear Stresses in Compressible Boundary Layers," *AIAA Journal,* Vol. 17, July 1979, pp. 736-744.

[13]Owen, F. K., Horstman, C. C., and Kussoy, M. I., "Mean and Fluctuating Flow Measurements in the Hypersonic Boundary Layer," *Journal of Fluid Mechanics,* Vol. 70, Pt. 2, 1975, pp. 393-413.

[14]Laderman, A. J. and Demetriades, A., "Mean and Fluctuating Flow Measurements in the Hypersonic Boundary Layer Over a Cooled Wall," *Journal of Fluid Mechanics,* Vol. 63, Pt. 1, 1974, pp. 121-144.

Elimination of Temperature Stratification in a Low-Speed Open-Return Wind Tunnel

J. M. Cimbala* and W. J. Park†
Pennsylvania State University,
University Park, Pennsylvania

Introduction

AIR in an enclosed room may be stratified, with warm air near the ceiling and cooler air near the floor. In cases where an open-return wind tunnel is operating in a room, this stratification can lead to significant measurement errors, especially when using hot-wire anemometry at low speeds. Even a relatively small temperature stratification near the inlet can be amplified several times in the contraction section of the wind tunnel.

This situation was observed to occur in the low-speed, open-return tunnel shown schematically in Fig. 1. The test section is 300 × 970 mm in cross section and 2.44 mm long, with a free-stream velocity range up to 15 m/s. The room housing the facility is heated by steam radiators. At low tunnel speeds, the air motion induced by the wind tunnel itself is not sufficient to

Received July 5, 1988; revision received Aug. 8, 1988.

*Assistant Professor, Department of Mechanical Engineering. Member AIAA.

†Graduate Assistant, Department of Mechanical Engineering.

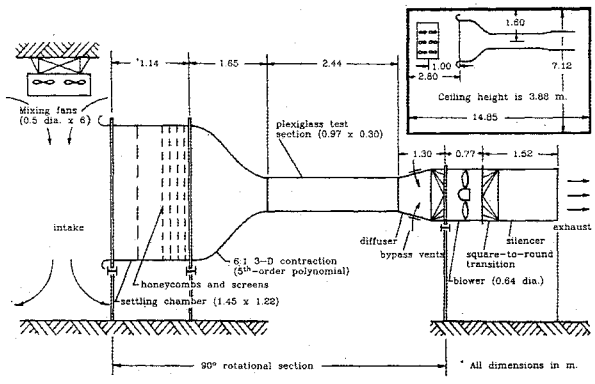

Fig. 1 Wind-tunnel schematic and position in room (inset).

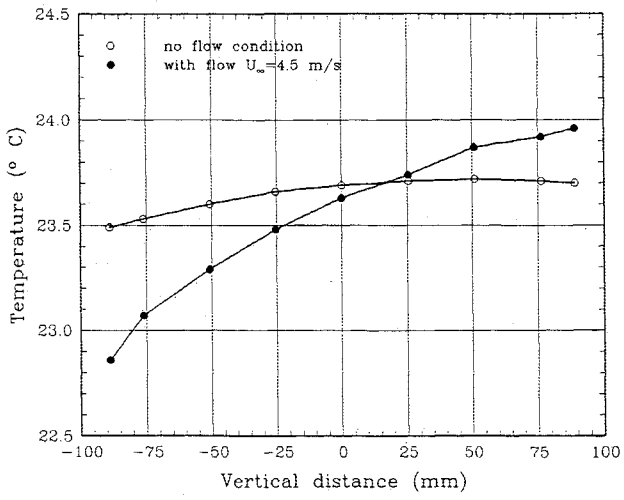

Fig. 2 Typical temperature gradients in a wind tunnel with and without flow.

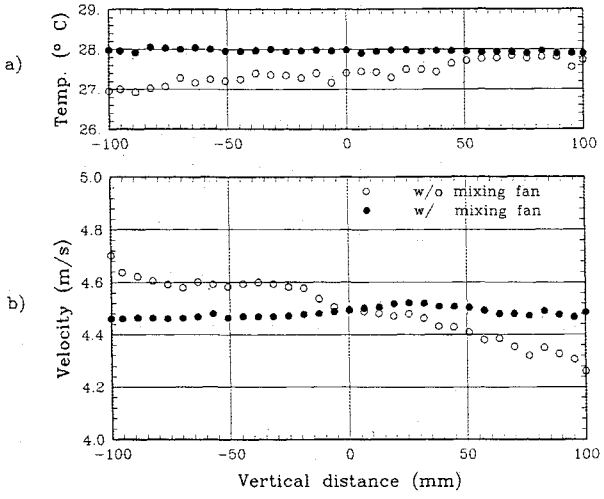

Fig. 3 Freestream velocity and temperature profiles.

mix the room air adequately. In the winter months, a temperature difference of several degrees Celsius from floor to ceiling is not uncommon.

Typical vertical temperature stratifications in the test section are illustrated in Fig. 2 for cases with and without flow through the wind tunnel. The sensor (Omega model 44204) was composed of two thermistors packaged in a miniature 2-mm-diam sensing head and had an accuracy of ±0.15°C. Since the instrument had a time constant of 10 s in still air, the readings were averaged over periods of 40 s. The vertical temperature difference across 200 mm of the test section was about 0.3°C in still air conditions. With a freestream velocity of 4.5 m/s, the temperature difference increased by a factor of almost 4, i.e., to about 1.1°C. The reason for this increase is that air is sucked in over the entire inlet, whose vertical height (1.22 m) is approximately four times that of the test section (0.3 m).

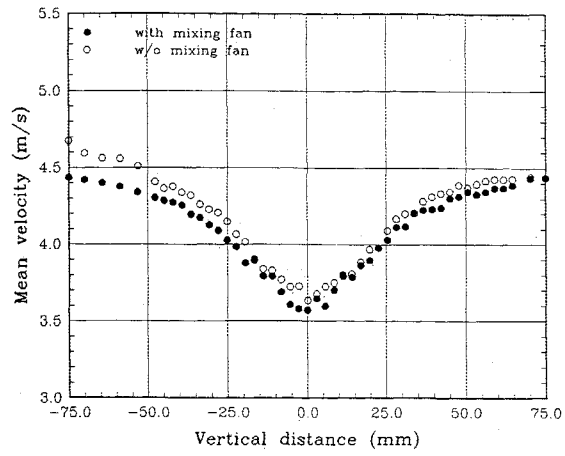

Fig. 4 Mean velocity profiles (two-dimensional cylinder wake at $x/d=20$, $Re_d=7000$).

Wind-Tunnel Inlet Modification

To eliminate this temperature stratification, a mixing fan assembly was installed just in front of the wind tunnel (Fig. 1). It was composed of six 0.5-m-diam electric fans suspended over the air intake area so as to mix the room air from top to bottom. The total volume flow rate of the fan assembly is approximately 8 m^3/s, which is about six times the tunnel volumetric flow rate of 4.5 m/s. Figure 3a shows the temperature variations in the vertical direction for typical cases with and without the mixing fan. As can be seen, the mixing fan virtually eliminates the temperature stratification by thoroughly mixing the air near the inlet.

To demonstrate the effect of the inlet mixing fan, mean velocity profiles for a uniform stream and a two-dimensional cylinder wake flow were obtained with a single hot-wire probe. In Fig. 3b, velocity profiles for the uniform stream at $U_\infty=4.5$ m/s are presented for cases with and without the inlet mixing fan. The hot wire was calibrated just prior to the profile measurement and at the centerline of the test section. Because of the temperature stratification, a "pseudoshear" profile was observed for the case without the inlet mixing fan. However, the case with the mixing fan shows that the flow is actually a uniform freestream without shear. The overall vertical temperature gradient inside the test section was approximately 5.0°C/m in this case, and this gradient produced about ±4.4% error in velocity.

In Fig. 4, the temperature stratification effect is illustrated in the wake behind a two-dimensional cylinder, measured with a single hot-wire probe at $Re_d=7000$ and at $x/d=20$. The hot-wire anemometer was calibrated before and after the survey to minimize the temporal temperature dependency of the hot-wire calibration. Again, the case without the mixing fan shows a somewhat sheared profile compared to the case with the mixing fan, as a result of temperature stratification errors introduced into the hot-wire measurements. We refer to it as a "pseudoshear," since the actual profile has no shear at all.

The inlet mixing fans did not affect the flow quality of the facility. No measurable increase in turbulence level of the wind tunnel or swirl effects were detected in the test section when the inlet mixing fan was added. Note that the settling chamber of the tunnel has several screens and honeycombs, designed according to turbulence-management suggestions of Loehrke and Nagib.[1] The turbulence intensity is about 0.1-0.2% at $U_\infty=5$ m/s.

Conclusions

Temperature stratification can be a significant source of error during hot-wire measurements in low-speed, open-return wind tunnels operating in an enclosed room. Errors of 4–5% in mean velocity measurements were observed at low (≈ 5 m/s) flow speeds in the tunnel of Fig. 1. The stratification could be eliminated by thoroughly mixing the air just upstream of the wind-tunnel inlet. Since the facility is equipped with adequate turbulence management (honeycombs and screens), the mixing was accomplished without reduction of flow quality.

Reference

[1]Loehrke, R. I and Nagib, H. M., "Experiments on Management of Freestream Turbulence," AGARD-R-598, 1972.

Parallelism in the Solution of Large Full Linear Systems Using a Matrix Partition Approach

Robert Morris Hintz*
General Microelectronics Corporation, San Diego, California

SOLUTION-TIME and data-storage requirements for the solution of full linear systems have become increasingly unwieldy with problem growth. Solution time for a 20,000-order complex system is about 1 day at 250 megaflops (millions of floating-point operations per second), and the data-storage requirements exceed 800 million words. Real systems require about a quarter of the solution time of complex and half the storage. Solution time is approximately proportional to the cube of problem size and storage requirements to the square of problem size. Thus, larger problems become even more intractable at an alarming rate.

Two parallel solution algorithms are proposed that can greatly decrease the solution time of full systems by employing multiple processes in the problem solution. Furthermore, the algorithms lend themselves to extremely efficient operation on disk resident problems because of benign demands on data transfer to and from disk. The basis for the algorithms is LU decomposition with partial row pivoting.[1] It is recommended that pivoting be used only sparingly because it can dramatically retard the performance of the algorithms. The parallel algorithms presented here do not include pivoting strategy.

The linear system to be solved is given by

$$Ax = b \tag{1}$$

where A is a full coefficient matrix, x and b are vectors, and the solution x is required, given A and b. Using LU decomposition, a nonsingular A matrix may be factored into the product of a lower and upper triangle matrix, as given in Eq. (2)[1]:

$$A = LU \tag{2}$$

where solution x then can be determined from the two-stage forward reduction (or forward elimination[1]) and back substitution.[1] The great bulk of the numerical effort is in the factoring algorithm, and multiple solutions may be easily obtained once A is factored.

The focus here is the decomposition of the A matrix using the matrix partition approach discussed in Ref. 2. The decomposition is implemented by partitioning the A matrix into square submatrices. Boundary partitions at the lower and right edges of A are, in general, not square. The partition-factoring algorithm[2] is restated as Eqs. (3a) and (3b). The diagonal partition submatrices L_{ii} and U_{jj} of

$$L_{ii}U_{ij} = A_{ij} - \sum_{k=1}^{i-1} L_{ik}U_{kj} \qquad i \le j \tag{3a}$$

$$L_{ij}U_{jj} = A_{ij} - \sum_{k=1}^{j-1} L_{ik}U_{kj} \qquad i > j \tag{3b}$$

Equations (3) are triangular, and all other submatrices are either square or rectangular. The solution of Eqs. (3) consists of a series of matrix multiplication and subtraction operations (to form $A - LU$ terms), followed the solution of a triangular system. More specifically, when $i = j$, the triangular system of Eq. (3a) is a factoring solution; when $i \neq j$, the triangular system of Eq. (3a) is a forward reduction, and the triangular system of Eq. (3b) is the transpose of a forward reduction.

The maximum partition size of the submatrices of Eqs. (3) is limited only by the amount of main data memory available to a computer at execution time. The technique thus lends itself to mapping large disk resident problems into an assemblage of in-core problems. Systems such as the order 20,000 problem previously discussed can be solved in a few million words of memory with negligible loss to input/output (I/O) when using concurrent computation and I/O.

In fact, a principal advantage of this technique is the very large computational effort generated per I/O request for a disk resident problem. Algorithm I/O can be structured to yield a full partition matrix multiply for each partition matrix read.[2] In other words, for complex arithmetic, $8m^3$ floating-point operations can be generated per $2m^2$ words read for a partition size of m. This translates to $4m$ floating-point operations per word of I/O, which gives a tremendous advantage to an I/O device supplying input to a computer concurrently with computation. These I/O efficiencies, coupled with the inherent parallelism of the partition algorithms, makes them extremely attractive.

The parallel factoring algorithm is developed here for both order n processes and order n^2 processes. Throughput of an order n^3 process operated on by order n processes is order n^2; an order n^3 process operated on by order n^2 processes is order n. The parallel algorithms are developed with each parallel set of processes collected in a group denoted as a step. All operations within a step may be executed in parallel with minor exceptions as noted.

First, the algorithm is parallelized with order n processes. The solution steps 1–n are given as follows.

Step 1: $i = 1$ in Eq. (3a), $j = 1$ in Eq. (3b) ($2n - 1$ processes):

$$L_{11}U_{11} = A_{11}$$

then, for the first row and column of partitions,

$$L_{11}U_{1j} = A_{1j}, \qquad j = 2,3,\ldots,n$$

$$L_{i1}U_{11} = A_{i1}, \qquad i = 2,3,\ldots,n$$

Step 2: $i = 2$ in Eq. (3a), $j = 2$ in Eq. (3b)† ($2n - 3$ processes):

$$L_{22}U_{2j} = A_{2j} - L_{21}U_{1j}, \qquad j = 2,3,\ldots,n$$

$$L_{i2}U_{22} = A_{i2} - L_{i1}U_{12}, \qquad i = 3,4,\ldots,n$$

Received March 1, 1988; revision received Sept. 6, 1988.

*Senior Applications Engineer.